Intuitive Interface for the Quantitative Evaluation of Speckle Patterns for Use in Digital Image and Volume Correlation Techniques

Jonathan B. Estrada
School of Engineering,
Brown University,
Providence, RI 02912
e-mail: jonathan_estrada@brown.edu

Christian Franck[1]
Assistant Professor
Mem. ASME
School of Engineering,
Brown University,
Providence, RI 02912
e-mail: franck@brown.edu

Digital image correlation (DIC) and digital volume correlation (DVC) are powerful means of resolving local kinematic descriptions of material deformation fields across a variety of material and testing platforms. Their spatial resolution, sensitivity, and accuracy depend in large part on the quality of the intrinsic material speckle pattern. Traditional evaluation of speckle pattern quality, or subset intensity distribution, relies on a set of well-characterized experimental measurements including rigid-body translation and rotation. In order to provide a significantly faster quantitative evaluation process on whether a particular speckle pattern is suitable for DIC or DVC purposes, we present a simple, intuitive DIC and DVC speckle pattern graphical user interface (GUI) tool programmed in MATLAB. This tool assesses the DIC and DVC robustness of user-supplied speckle patterns via a two-step procedure: The first step involves warping the specific image according to a set of analytically prescribed deformation functions. The second step involves correlating the analytically warped and reference image pairs to recover the prescribed displacement field and its quantitative comparison to the prescribed warping function. Since the accuracy and precision of the recovered solution depend on the characteristics of the intensity distributions encoded in the image, this approach allows for a simple, yet effective, quantification procedure of the correlation suitability in the supplied image speckle pattern. In short, this procedure allows for fast and quantitative evaluation of the quality and suitability of a given speckle pattern to be used in DIC and DVC applications without the need of performing time-consuming experimental measurements. As such, we hope that this free tool will benefit anyone interested in performing DIC- or DVC-based kinematic measurements. [DOI: 10.1115/1.4030821]

Introduction

The last three decades have shown a tremendous increase in the use of noncontact experimental imaging techniques due to the wider accessibility of high-resolution cameras and low-cost computing power [1–3]. DIC and its volumetric extension, and DVC have provided significant insight into the deformation behavior of various material classes (e.g., from ceramics to hydrogels) across a broad range of length and time scales [4–14]. In particular, experimental applications of DIC and DVC for resolving spatially varying displacement and strain fields have spurred the development of various levels of sophistication in built-in motion capturing algorithms [9,15–19]. Equally exciting are recent endeavors to provide free, open-source access of digital image and volume correlation code packages to a broad spectrum of end users [15,20–24].

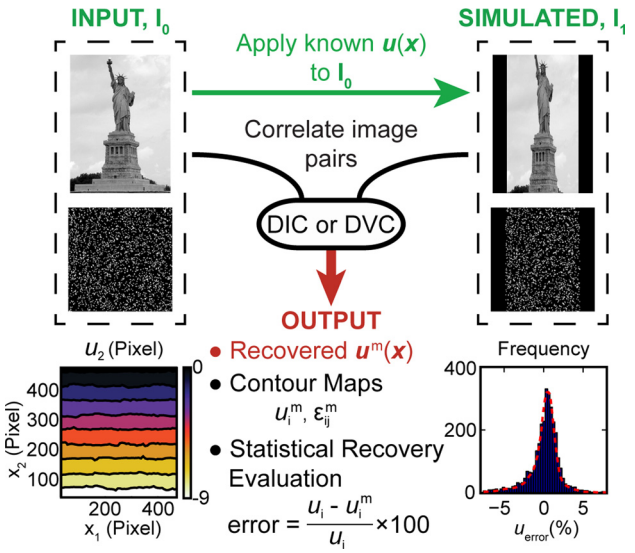

Fig. 1 Schematic overview of the DIC and DVC simulators

Successful correlation of image subsets, or estimation of the kinematic motion fields between successive images, relies in large part on the particular subset intensity profiles and their gradients, known as speckle patterns [1,3]. Denser, more gray-valued speckle patterns generally correlate better, providing higher spatial displacement resolution and sensitivity compared to repeat patterns or large areas of constant intensity [3,14,15,17,25–27]. Since many materials employed in DIC and DVC investigations do not inherently possess high-quality speckle patterns, researchers have introduced various levels of sophistication in fabricating high-quality DIC and DVC speckle patterns. As such, almost every DIC or DVC experiment begins with a set of simple speckle pattern characterization tests to benchmark the maximum displacement resolution sensitivity at hand. These tests typically involve simple rigid-body motions, such as rigid-body translation or rotation. The goal is to quantitatively compare the imposed motion with the recovered motion estimates from DIC or DVC. Although the experiments themselves are relatively straightforward, depending on the material in use, significant amounts of time and effort might be spent on generating reproducible and appropriate speckle patterns, resulting in a large number of required samples and evaluation tests.

In order to significantly reduce the material and time burden associated with this procedure, this paper presents an intuitive, open-source, MATLAB-based interface for characterizing and optimizing a particular material speckle pattern. The purpose of our tool is to replace the traditionally experimentally run calibration tests with a set of software-based quantitative simulations, which are freely accessible via our website[2]. The working principle is schematically illustrated in Fig. 1. Here, the user-supplied reference image undergoes a series of simulated deformations to produce a set of analytically warped images (top row, Fig. 1). Each image pair, consisting of the reference (true) and synthetically deformed (warped) image, is then cross-correlated to obtain the full-field motion estimate between the images (middle row, Fig. 1). Finally, the recovered displacement fields for each deformation scenario are represented as displacement contour maps,

[1]Corresponding author.

Contributed by the Applied Mechanics Division of ASME for publication in the JOURNAL OF APPLIED MECHANICS. Manuscript received May 1, 2015; final manuscript received June 8, 2015; published online June 25, 2015. Editor: Yonggang Huang.

[2]http://franck.engin.brown.edu/~christianfranck/FranckLab/Home.html.

and the recovery error is computed (bottom row, Fig. 1). The set of standard displacement warping functions, which is described in detail in the Methods section, includes rigid-body translation, uniaxial tension, pure shear, and the resulting displacement field due to application of a point force acting on an elastic half-space.

Methods

The GUI for each DIC and DVC simulator provides simple and intuitive access for evaluating the speckle pattern quality in the user-specific image. Figure 2 provides a snapshot of the DIC GUI. Since the DVC GUI is similarly structured in comparison to the DIC interface, with the main difference being the addition of the third (x_3, u_3) dimension, the reader should be able to extrapolate any descriptions of the DIC interface onto the DVC GUI, which we purposefully omit here for the sake of brevity.

The GUI. The DIC GUI is compartmentalized into three (top, middle, and bottom) organizational rows (Figs. 2(*a*), 2(*b*)–2(*d*), and 2(*e*) and 2(*f*), respectively). The input parameters in Fig. 2(*a*) allow the user to upload an image in.*tif,.jpg,.bmp*, or.*mat* format, and to select the typical DIC algorithm parameters, such as interrogation (subset) window size, w, and spacing, d. The subset size, w, specifies the amount of intensity information to be correlated in each subset, which in turn determines the highest resolvable spatial frequency via DIC. The subset spacing, d, determines the spatial resolution of the resulting DIC displacement grid. Although small values of d lead to high spatial grid resolution, the maximally resolvable spatial feature size (i.e., the highest intrinsic spatial frequency) depends primarily on w, not d [28–31]. Computationally, increasing d and/or decreasing w leads to a significant decrease in processing time. Due to practical limitations, most correlation studies employ subset window sizes ranging from 32 to 64 pixels, as a compromise between the amount of resolvable spatial frequency content and a robust image motion estimate. Further information regarding the effect of correlation subset window size and spacing on the final DIC or DVC resolutions can be found elsewhere [3,15,24].

Next, the user specifies the nominally applied transformation strain, ε_t, which is used to scale the relative amount of introduced image warping into the uploaded user image. It is important to note that the featured DIC and DVC simulator algorithms do not include higher-order shape functions, and thus it is strongly recommended to limit the level of transformation strain, ε_t, to within 10%. The next text box allows the user to specify the amount of horizontal pixel translation of the reference image. Again, since the formalism in the DIC and DVC algorithms utilize the same Eulerian cross-correlation frames, maximum pixel shifts should

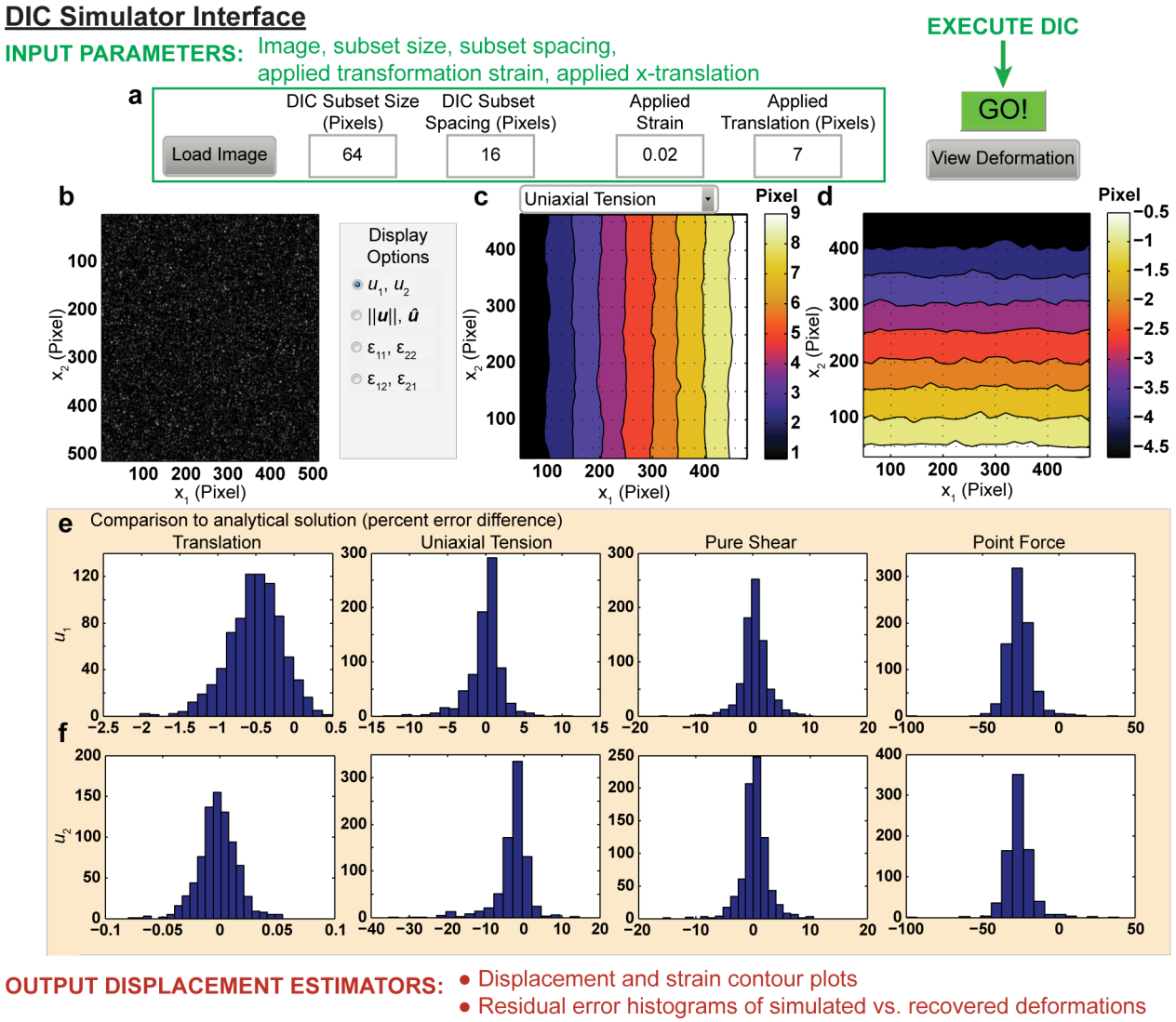

Fig. 2 Screenshot of the MATLAB-based DIC simulator GUI, with (*a*) input parameters, (*b*) input image, and output (*c*), (*d*) contour maps and (*e*), (*f*) residual deformation recovery error histograms

be limited to stay within half of the subset size ($w/2$) to maintain robust correlation. Once all text fields within the top row of the GUI have been appropriately populated, the "GO" button executes the simulator. After the simulator is executed, the user may select "View Deformation" to display and save both reference and deformed image pairs as well as the displacement component fields for each deformation case. Options to save resulting image deformation and simulated displacement data include as pictures in ".tif" format and numerically into variables as "imagedata.mat" and "dispdata.mat" files in the working directory.

The middle row features graphical outputs of the uploaded image by the user (Fig. 2(*b*)), and user-selected color contour plots of the recovered displacement or strain fields using DIC (Figs. 2(*c*) and 2(*d*)). Color contour plot data use a modified CMR map suitable for both black-and-white and color viewing [32]. The user-specified output variables are selected from a predefined radio button menu and displayed in pixels with intensities rendered as color-coded contour maps. Possible graphical contour outputs include the horizontal (u_1) and vertical (u_2) displacements, as well as individual components of the infinitesimal strain tensor, ε_{ij}. The bottom row of the GUI represents a series of histograms quantifying distributions of the DIC displacement recovery error, which is defined as

$$\text{recovery error } (\%) = \frac{u_i - u_{im}}{u_i} \times 100 \tag{1}$$

where u_i and u_{im} represent the analytically imposed and DIC-recovered (measured) displacements, respectively. Each histogram represents the recovery error for a given applied deformation mode (e.g., uniaxial tension) per given displacement (u_1 versus u_2). The purpose of plotting recovery error is twofold. First, visual inspection of the error distribution provides quantitative information about the speckle-dependent DIC accuracy and precision, represented by the mean and the spread of the distribution, respectively, of the recovered solutions. Second, the amount of outliers provides information as to how much of the speckle intensity patterns are suitable for DIC or DVC purposes, i.e., a significant amount of outliers with respect to the total population of data points indicates that large portions of the image are not suitable for DIC use. In many images such areas correspond to areas of constant intensity over which the intensity gradient is zero, leading to poor cross-correlation [3,25]. As part of the downloadable simulator package[2], we supply the user with a high-quality speckle image that exhibits very good DIC displacement recovery properties, which provides a reference for the statistical evaluation procedure for the unfamiliar user.

Simulated Deformation Fields. As shown in Fig. 1, the first step in the image evaluation procedure begins by mapping the intensity values from the reference image to a synthetically deformed image of equal size using MATLAB's built-in "interp3" and "interp2" functions for DVC and DIC, respectively. The mapping procedure in the DIC simulator is performed using the following four displacement field functions:

$$u_i = u_0 \cdot \delta_{i1} \tag{2}$$

$$u_i = \varepsilon_t[(x_1 - x_{10})\delta_{i1} - \nu(x_2 - x_{20})\delta_{i2}] \tag{3}$$

$$u_i = \varepsilon_t[(x_1 - x_{10})\delta_{i2} + (x_2 - x_{20})\delta_{i1}] \tag{4}$$

$$u_i = \frac{1+\nu}{2\pi E}\left\{\frac{2(1-\nu)r + x_3}{r(r+x_3)}P_i + \frac{2r(\nu r + x_3) + x_3^2}{r^3(r+x_3)^2}x_i \cdot (x_i P_i)\right\} \tag{5}$$

where ε_t is the applied transformation strain, δ_{ij} is the Kroneker delta, $r = \sqrt{x_i x_i}$ with $i = 1, 2$ (planar motion), and each $\mathbf{u}(\mathbf{x})$ describes either rigid-body motion (Eq. (2)), uniaxial tension (Eq. (3)), pure shear (Eq. (4)), or a point force, $\mathbf{P}$, acting tangent to an elastic halfspace (Eq. (5)) [33]. The Poisson's ratio, ν, is set to 0.45 for all deformation cases. The ratio of the material-normalized point force components in all directions P_i to the Young's modulus E in Eq. (5) is taken to be the transformation strain ε_t, or $P_i/E = \varepsilon_t(\delta_{i1} + \delta_{i2})$. The original (reference) image and the synthetically deformed image constitute a respective deformation image pair, which is analyzed using DIC. The volumetric DVC simulator employs 3D extensions of the displacement functions given by Eqs. (2)–(4), with the exception that the 2D Boussinesq problem is replaced by a point force acting in an infinite medium [34], for which the displacement components are given by

$$u_i = \frac{1+\nu}{8\pi E(1-\nu)r}\left\{\frac{x_k x_i}{r^2}P_k + (3-4\nu)P_i)\right\} \tag{6}$$

where $i = 1, 2, 3$ (3D motion). The Poisson's ratio is identical to the value used in Eq. (5), and the magnitude of the material-normalized point force, $\mathbf{P}/E$, is $P_i/E = \varepsilon_t\delta_{i3}$.

Digital Image and Volume Correlation Algorithm. Both DIC and DVC simulators make use of our previously developed fast Fourier transform based correlation algorithm [35]. The analytical formulation behind both algorithms is identical and can be written in typical cross-correlation form

$$c(\mathbf{u}) = \int_{\Omega_x} f(\mathbf{x})g(\mathbf{x}+\mathbf{u})d\Omega_x \tag{7}$$

where $c(\mathbf{u})$ is the cross-correlation coefficient, and $f(\mathbf{x})$ and $g(\mathbf{x})$ denote the image intensities in the reference and deformed image subsets, Ω_x. The displacement vector, $\mathbf{u}(\mathbf{x})$, between the two subsets is determined by the argmax$(c(\mathbf{u}))$. The main difference between the code structures of the DVC and DIC algorithms is that DVC uses cubic subsets and volumetric images in 3D voxel space, whereas the DIC uses square subsets in 2D pixel space. Both algorithms feature subpixel resolution capability [35]. This type of DIC and DVC formulation presents the simplest implementation and lowest order motion reconstruction—with two and three degrees-of-freedom (DoF) in DIC and DVC, respectively—based on rigid-body translation of individual subsets. Since the goal of the overall simulator is to provide the end-user a general, zeroth order estimate about the DIC/DVC quality of their speckle pattern, we believe that the use of such a simple, yet fast motion algorithm is justified. If the user requires higher fidelity motion reconstruction, we suggest utilization of already available higher-order DIC and DVC algorithms [2,15,18,24].

Results

To gain a better understanding of the typical output generated by either DIC or DVC simulator, Fig. 3 provides a graphical example. As described in detail in the Methods section, two user-specified images (Figs. 3(*a*) and 3(*f*)) are uploaded and deformed according to Eqs. (2)–(5). For our illustration purposes here, we focus on uniaxial tension (Figs. 3(*b*), 3(*c*), 3(*g*), and 3(*h*)) and the applied point force (Figs. 3(*d*), 3(*e*), 3(*i*), and 3(*j*)) serving both as examples of uniform strain and concentrated strain deformation cases. First examining the results from the uniaxial tension deformation mode, it is clear that the image with the more specklelike features provides the most accurate reconstruction (Fig. 3(*b*)) of the uniaxially applied motion. This is highlighted by the linearly varying contour plot of the u_2 (vertical) displacement field. Similarly, the recovered displacement error is normally distributed with a mean, μ, of -0.154% and standard deviation, σ, of 2.39% (Fig. 3(*c*)).

When comparing the displacement contour results of u_2 recovered from the Statue of Liberty image to the image possessing a well-defined speckle intensity pattern, the Statue of Liberty image

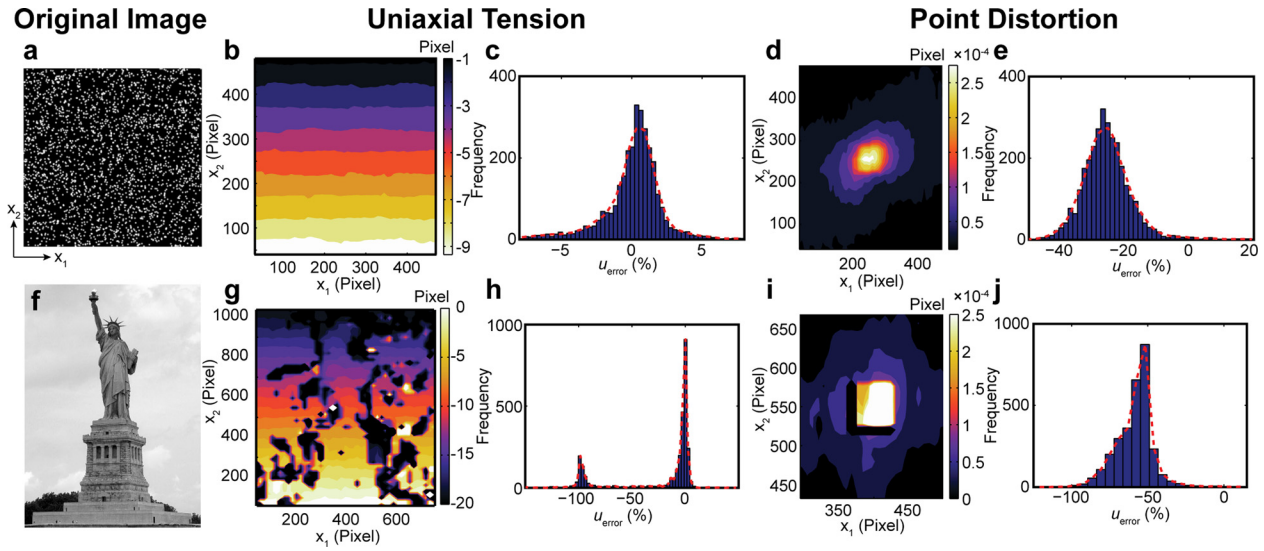

Fig. 3 Example (*a*) and (*f*) input images and output displacement contour maps and residual error histograms in (*b*), (*c*), (*g*), and (*h*) uniaxial tension and (*d*), (*e*), (*i*), and (*j*) for a point force

is able to provide reasonable displacement estimates in areas of varying grayscale intensities but to a much lesser extent in areas of similar intensity magnitudes. Local areas of constant intensity lead to poor correlation due to a vanishing local intensity gradient [3], which is highlighted by the degraded displacement information shown in Fig. 3(*g*). General uniaxial displacement behavior is observed in the contour image, and whereas some areas within the image correlate well and provide the proper displacement reconstructions, others produce significant error in their estimate. The considerable error is reflected in the cumulative recovery error distribution (Fig. 3(*h*)), which shows a bimodal error distribution. One of the peaks is centered around a mean value close to zero ($-2.92\pm30.9\%$) corresponding to the areas in the images of well-defined grayscale intensity gradients, whereas the other, smaller, peak is centered close to 100% error representing the areas of poor correlation in the image.

The displacement recovery results from the analytical point force solution applied to both the speckled and Statue of Liberty images display a higher degree of error due to underresolved displacement gradients near the point force. Here, the spatial differences between the recovered displacement fields in Figs. 3(*d*) and 3(*i*) are primarily due to the differences in the intensity distribution of the image-respective subsets. Additional error is introduced by the inability of the simple DIC algorithm to properly resolve the local displacement gradients near the applied point force. This is explains why the speckled image carries a displacement recovery error of $-26.4\pm8.48\%$ (Fig. 3(*e*)) albeit the high-quality subset textures. Upgrading the DIC algorithm to include higher-order shape functions will significantly reduce this error estimate by resolving higher spatial frequency content in the displacement fields [18,24]. Nevertheless, the recovered displacement contour image (Fig. 3(*e*)) portrays the qualitatively correct shape and distribution of the analytically imposed displacement field. The Statue of Liberty image, on the other hand, contains various vertical and horizontal features of similar intensities, which lead to poor cross-correlation and the resulting squarelike shape of the point force displacement solution with a recovery error of $-62.3\pm30.7\%$ (Fig. 3(*j*)), which are significantly more degenerate in comparison to the high-quality speckle image results (Fig. 3(*e*)).

Conclusions

In this manuscript, we present a simple GUI for the evaluation of image intensity (speckle) patterns for use in DIC or DVC applications. Using the GUI, the user first uploads an image, which then undergoes a series of analytically imposed deformation functions, which are subsequently recovered via DIC or DVC. Computation of the displacement recovery error (Eq. (1)) provides a quantitative assessment of the correlation-appropriateness of the intrinsic image speckle patterns (Fig. 3). Our simulator tool allows for a simple, fast, and effective speckle pattern evaluation procedure, which traditionally is handled using a series of time- and/or material-consuming experimental measurements. Furthermore, while the current GUI version supports four different displacement functions as DIC and DVC benchmark tests, it is relatively straightforward to incorporate additional or any user-specific analytical displacement functions within the MATLAB-based framework of the GUI itself. This should provide the end-user with significant flexibility. When using the GUI to evaluate the quality of the speckle pattern at hand, there are several current limitations that should be noted. First, for images at resolutions below 512×512 pixels (DIC) or $512\times512\times96$ voxels (DVC), only small deformations (<10%) should be applied due to increasing accumulation of interpolation bias during the image warping process. This is so because the current image warping process relies on linearly interpolating the image intensities from the reference into the deformed configuration. If the original image is of low resolution (e.g., 128×128 pixels^2) and the user applies large strains (>10%), a significant amount of interpolation is required to map the image intensities from the reference into the deformed configuration producing significant amounts of interpolation bias, or image artifacts. Second, simulation of finite deformations (>10%) should also generally be avoided, since the current DIC and DVC formalism only capture rigid-body translation (2DoF and 3DoF in DIC and DVC, respectively) at the subset level. Large deformation simulations would require upgrading the current DIC and DVC algorithms, which can be achieved using already existing packages [2,15,18,24] but is beyond the current work. Last, should the user decide to proceed with using DIC or DVC for his or her research purposes, we strongly recommend using more sophisticated and hence accurate DIC and DVC algorithms, which are freely available from our website[2] and elsewhere [15,20–24].

In conclusion, the presented speckle pattern evaluation GUI provides a simple and effective methodology for quantitatively determining whether a certain image or volume stack is suited for DIC or DVC purposes. In addition to providing free access to our software online[2], we are also currently working on a mobile phone device application, which will allow speckle pattern evaluation directly at the workbench without the need of a computer, simply

by taking an image on one's mobile phone. We hope that these open-platform tools will provide the mechanics community with a fast, efficient, and quantitative approach to performing DIC and DVC measurements.

Acknowledgment

We acknowledge Soonsung Hong for the development of the original FFT-based DIC algorithm, Eyal Bar-Kochba for technical assistance with the preparation of this manuscript, and the broader mechanics community for the valuable and positive feedback in regards to the DIC and DVC GUI developments.

References

[1] Hild, F., and Roux, S., 2012, *Digital Image Correlation*, Wiley-VCH, Weinheim, Germany.
[2] Gates, M., Lambros, J., and Heath, M. T., 2011, "Towards High Performance Digital Volume Correlation," Exp. Mech., **51**(4), pp. 491–507.
[3] Sutton, M. A., Orteu, J. J., and Schreier, H., 2009, *Image Correlation for Shape, Motion and Deformation Measurements: Basic Concepts, Theory and Applications*, Springer, New York.
[4] Du, Y., Diaz, F. A., Burguete, R. L., and Patterson, E. A., 2011, "Evaluation Using Digital Image Correlation of Stress Intensity Factors in an Aerospace Panel," Exp. Mech., **51**(1), pp. 45–57.
[5] Blaber, J., Adair, B. S., and Antoniou, A., 2015, "A Methodology for High Resolution Digital Image Correlation in High Temperature Experiments," Rev. Sci. Instrum., **86**(3), p. 035111.
[6] Grassi, L., Väänänen, S. P., Yavari, S. A., Jurvelin, J. S., Weinans, H., Ristinmaa, M., Zadpoor, A. A., and Isaksson, H., 2014, "Full-Field Strain Measurement During Mechanical Testing of the Human Femur at Physiologically Relevant Strain Rates," ASME J. Biomech. Eng., **136**(11), p. 111010.
[7] Toyjanova, J., Flores-Cortez, E., Reichner, J. S., and Franck, C., 2015, "Matrix Confinement Plays a Pivotal Role in Regulating Neutrophil-Generated Tractions, Speed and Integrin Utilization," J. Biol. Chem., **290**(6), pp. 3752–3763.
[8] Ambu, R., Aymerich, F., and Bertolino, F., 2005, "Investigation of the Effect of Damage on the Strength of Notched Composite Laminates by Digital Image Correlation," J. Strain Anal. Eng. Des., **40**(5), pp. 451–461.
[9] Bormann, T., Schulz, G., Deyhle, H., Beckmann, F., de Wild, M., Küffer, J., Münch, C., Hoffmann, W., and Müller, B., 2014, "Combining Micro Computed Tomography and Three-Dimensional Registration to Evaluate Local Strains in Shape Memory Scaffolds," Acta Biomater., **10**(2), pp. 1024–1034.
[10] Kim, K., and Daly, S., 2011, "Martensite Strain Memory in the Shape Memory Alloy Nickel-Titanium Under Mechanical Cycling," Exp. Mech., **51**(4), pp. 641–652.
[11] Coudrillier, B., Pijanka, J., Jefferys, J., Sorensen, T., Quigley, H. A., Boote, C., and Nguyen, T. D., 2015, "Collagen Structure and Mechanical Properties of the Human Sclera: Analysis for the Effects of Age," ASME J. Biomech. Eng., **137**(4), p. 041006.
[12] Abanto-Bueno, J., and Lambros, J., 2002, "Investigation of Crack Growth in Functionally Graded Materials Using Digital Image Correlation," Eng. Fract. Mech., **69**(14–16), pp. 1695–1711.
[13] Bay, B. K., Smith, T. S., Fyhrie, D. P., and Saad, M., 1999, "Digital Volume Correlation: Three-Dimensional Strain Mapping Using X-Ray Tomography," Exp. Mech., **39**(3), pp. 217–226.
[14] Kammers, A. D., and Daly, S., 2013, "Digital Image Correlation Under Scanning Electron Microscopy: Methodology and Validation," Exp. Mech., **53**(9), pp. 1743–1761.
[15] Bar-Kochba, E., Toyjanova, J., Andrews, E., Kim, K. S., and Franck, C., 2015, "A Fast Iterative Digital Volume Correlation Algorithm for Large Deformations," Exp. Mech., **55**(1), pp. 261–274.
[16] Madi, K., Tozzi, G., Zhang, Q. H., Tong, J., Cossey, A., Au, A., Hollis, D., and Hild, F., 2013, "Computation of Full-Field Displacements in a Scaffold Implant Using Digital Volume Correlation and Finite Element Analysis," Med. Eng. Phys., **35**(9), pp. 1298–1312.
[17] Schreier, H. W., and Sutton, M. A., 2002, "Systematic Errors in Digital Image Correlation Due to Undermatched Subset Shape Functions," Exp. Mech., **42**(3), pp. 303–310.
[18] Lu, H., and Cary, P. D., 2000, "Deformation Measurements by Digital Image Correlation: Implementation of a Second-Order Displacement Gradient," Exp. Mech., **40**(4), pp. 393–400.
[19] Poissant, J., and Barthelat, F., 2010, "A Novel 'Subset Splitting' Procedure for Digital Image Correlation on Discontinuous Displacement Fields," Exp. Mech., **50**(3), pp. 353–364.
[20] Eberl, C., 2010, "Digital Image Correlation and Tracking," The MathWorks Inc., Natick, MA, http://www.mathworks.com/matlabcentral/fileexchange/12413-digital-image-correlation-and-tracking
[21] Jones, E., 2013, "Improved Digital Image Correlation (DIC)," The MathWorks Inc., Natick, MA, http://www.mathworks.com/matlabcentral/fileexchange/43073-improved-digital-image-correlation–dic-
[22] Tseng, Q., Duchemin-Pelletier, E., Deshiere, A., Balland, M., Guillou, H., Filhol, O., and Théry, M., 2012, "Spatial Organization of the Extracellular Matrix Regulates Cell–Cell Junction Positioning," Proc. Natl. Acad. Sci., **109**(5), pp. 1506–1511.
[23] Mori, N., and Chang, K. A., 2003, "Introduction to MPIV," http://www.oceanwave.jp/softwares/mpiv/
[24] Blaber, J., Adair, B., and Antoniou, A., 2015, "Ncorr: Open-Source 2D Digital Image Correlation Matlab Software," Exp. Mech., **55**(6), pp. 1105–1122.
[25] Bornert, M., Brémand, F., Doumalin, P., and Dupré, J. C., 2009, "Assessment of Digital Image Correlation Measurement Errors: Methodology and Results," Exp. Mech., **49**(3), pp. 353–370.
[26] Fazzini, M., Mistou, S., Dalverny, O., and Robert, L., 2010, "Study of Image Characteristics on Digital Image Correlation Error Assessment," Opt. Lasers Eng., **48**(3), pp. 335–339.
[27] Crammond, G., Boyd, S., and Dulieu-Barton, J., 2013, "Speckle Pattern Quality Assessment for Digital Image Correlation," Opt. Lasers Eng., **51**(12), pp. 1368–1378.
[28] Yuan, Y., Huang, J., Peng, X., Xiong, C., Fang, J., and Yuan, F., 2014, "Accurate Displacement Measurement Via a Self-Adaptive Digital Image Correlation Method Based on a Weighted ZNSSD Criterion," Opt. Lasers Eng., **52**, pp. 75–85.
[29] Eckstein, A., and Vlachos, P. P., 2009, "Assessment of Advanced Windowing Techniques for Digital Particle Image Velocimetry (DPIV)," Meas. Sci. Technol., **20**(7), p. 075402.
[30] Westerweel, J., Dabiri, D., and Gharib, M., 1997, "The Effect of a Discrete Window Offset on the Accuracy of Cross-Correlation Analysis of Digital PIV Recordings," Exp. Fluids, **23**(1), pp. 20–28.
[31] Huang, J., Pan, X., Peng, X., Yuan, Y., Xiong, C., Fang, J., and Yuan, F., 2013, "Digital Image Correlation With Self-Adaptive Gaussian Windows," Exp. Mech., **53**(3), pp. 505–512.
[32] Rappaport, C., 2002, "A Color Map for Effective Black-and-White Rendering of Color Scale Images," IEEE Antennas Propag. Mag., **44**(3), pp. 94–96.
[33] Landau, L. D., Pitaevskii, L. P., Kosevich, A. M., and Lifshitz, E. M., 2012, *Theory of Elasticity*, Elsevier, Burlington, MA.
[34] Bower, A. F., 2010, *Applied Mechanics of Solids*, CRC Press, Boca Raton, FL.
[35] Franck, C., Hong, S., Maskarinec, S. A., and Tirrell, D. A., 2007, "Three-Dimensional Full-Field Measurements of Large Deformations in Soft Materials Using Confocal Microscopy and Digital Volume Correlation," Exp. Mech., **47**(3), pp. 427–438.